**Aalborg Universitet**

AALBORG UNIVERSITY

# Indenting glasses with indenters of varying stiffness and sharpness

Christensen, Johan Frederik Schou; Krishnan, N. M. Anoop; Bauchy, Mathieu; Smedskjær, Morten Mattrup

*Published in:*
Journal of Non-Crystalline Solids

*DOI (link to publication from Publisher):*
10.1016/j.jnoncrysol.2022.122111

*Creative Commons License*
CC BY 4.0

*Publication date:*
2023

*Document Version*
Publisher's PDF, also known as Version of record

Link to publication from Aalborg University

*Citation for published version (APA):*
Christensen, J. F. S., Krishnan, N. M. A., Bauchy, M., & Smedskjær, M. M. (2023). Indenting glasses with indenters of varying stiffness and sharpness. *Journal of Non-Crystalline Solids*, *603*, Article 122111. https://doi.org/10.1016/j.jnoncrysol.2022.122111

**General rights**
Copyright and moral rights for the publications made accessible in the public portal are retained by the authors and/or other copyright owners and it is a condition of accessing publications that users recognise and abide by the legal requirements associated with these rights.

- Users may download and print one copy of any publication from the public portal for the purpose of private study or research.
- You may not further distribute the material or use it for any profit-making activity or commercial gain
- You may freely distribute the URL identifying the publication in the public portal -

**Take down policy**
If you believe that this document breaches copyright please contact us at vbn@aub.aau.dk providing details, and we will remove access to the work immediately and investigate your claim.

Downloaded from vbn.aau.dk on: December 04, 2025

Journal of Non-Crystalline Solids 603 (2023) 122111

Contents lists available at ScienceDirect

Journal of Non-Crystalline Solids

journal homepage: www.elsevier.com/locate/jnoncrysol

# Indenting glasses with indenters of varying stiffness and sharpness

Johan F.S. Christensen [a], N.M. Anoop Krishnan [b,c], Mathieu Bauchy [d], Morten M. Smedskjaer [a,*]

[a] Department of Chemistry and Bioscience, Aalborg University, Aalborg 9220, Denmark
[b] Department of Civil Engineering, Indian Institute of Technology Delhi, Hauz Khas, New Delhi 110016, India
[c] Yardi School of Artificial Intelligence, Indian Institute of Technology Delhi, Hauz Khas, New Delhi 110016, India
[d] Department of Civil and Environmental Engineering, University of California, Los Angeles, CA 90095, USA

ARTICLE INFO

*Keywords:*
Oxide glasses
Indentation
Crack initiation
Indentation size effect (ISE)

ABSTRACT

In this study, the effects of both indenter sharpness and stiffness on the indentation response of oxide glasses have been investigated. Using five different indenters, the indentation response in terms of glass deformation mechanism, cracking behavior, and hardness has been examined for three glasses (sodium silicate, sodium borate, and sodium borosilicate). For right square-based pyramidal diamond indenters with varying tip angle, increased indenter sharpness reduces the magnitude of the indentation size effect. Additionally, increased indenter sharpness lowers the crack initiation resistance, which is linked to a reduction of densification. For indenters with the same geometry but made of different materials, the effect of the indenter material is insignificant when the indenter is substantially stiffer than the specimen. When the stiffness of the indenter is only slightly higher or similar to that of the sample, substantial deformation of the indenter occurs, reducing the effective indenter sharpness and hence affecting the indentation response.

## 1. Introduction

In the study of mechanical properties of oxide glasses, the instrumented indentation technique can provide insights into a broad range of phenomena. Hardness [1], stiffness [2], crack initiation resistance [3], ability to densify [4], and indentation fracture toughness [5] are examples of properties that can be determined. Combined with the experimental simplicity of the technique that can enable fast, localized testing without extensive sample preparation, these advantages have made instrumented indentation testing very popular [5–7]. However, indentation results might be affected by, e.g., improper surface preparation, indenter imperfections, and variations in ambient temperature and humidity [1,8], thus indentation experiments should generally be performed carefully and caution should be used when comparing results from different sources.

The fundamental principle of indentation is to press a hard object (the indenter) into the surface of the softer material under examination and observe how the material responds. Indentation with sharp indenters induces permanent deformation of the material, hence leaving an imprint (indent) and potentially, if the applied load is sufficiently high, causing crack formation. As oxide glasses are brittle materials at the macroscale, it might appear surprising that indentation can produce permanent indents. However, oxide glasses can indeed deform plastically at the microscale, especially under the high stresses that can be attained when subjected to compressive stress [1]. Different types of deformation occur in oxide glasses during indentation, and these are typically categorized as either reversible elastic deformation or permanent (plastic) deformation. The latter can be further divided into densification and isochoric shear flow [9].

A key bottleneck for the application of oxide glasses is their relatively low strength [10], which is caused by surface cracks/flaws that lead to stress concentration upon an applied tensile stress. Such defects are inevitably formed during production and use of the glass material [11,12]. Thus, it is important to improve the damage resistance of oxide glasses to reduce the formation of such defects, or alternatively improve the damage tolerance, i.e., the resistance against growth of the defects. To this end, instrumented indentation testing is a valuable tool as it can generate surface cracks/flaws in a controlled manner and thus be used for the evaluation of damage resistance. Furthermore, damage tolerance can be estimated by indentation fracture toughness measurements, although it should be noted that evaluation of fracture toughness by indentation can be problematic [13]. Instrumented indentation testing can, at least for some glass applications, mimic real-life contact events that glass products experience during use. For example, it has been

* Corresponding author.
*E-mail address:* mos@bio.aau.dk (M.M. Smedskjaer).

https://doi.org/10.1016/j.jnoncrysol.2022.122111
Received 16 September 2022; Received in revised form 18 December 2022; Accepted 21 December 2022
0022-3093/© 2022 The Author(s). Published by Elsevier B.V. This is an open access article under the CC BY license (http://creativecommons.org/licenses/by/4.0/).

reported that surface damages generated by laboratory indentation experiments resemble those formed during real-life use of cover glasses on mobile devices [14]. Improved damage resistance has been realized in laboratory glasses with record-high resistance to crack initiation [15,16], but has also been commercialized into products such as Corning® Gorilla® Glass 3 with a high damage resistance as a result of composition optimization as well as ion exchange post-treatment [17].

Indentation experiments can be conducted under different conditions, including variations in the applied load, measurement atmosphere, indenter properties, etc. Such varying conditions have a considerable effect on the indentation response of the material, for which reason laboratory indentation experiments typically follow some standards or common practices. Still, it is highly relevant to understand how the experimental design parameters affect the results, as such knowledge can give a better understanding of how laboratory findings can be translated into improvements of real-life glass products. A key parameter for indentation experiments is obviously the choice of indenter. Several different indenter types are commonly used in the study of oxide glasses, especially Vickers, Knoop, Berkovich, and cube-corner indenters. Microhardness measurements are commonly performed using a Vickers or Knoop indenter, which both have four-sided pyramid geometries [18,19], with the Vickers indenter being the most frequently used [5]. The Vickers indenter has the geometry of a right square-based pyramid with a tip angle ($\alpha$) of 136°, where $\alpha$ is the angle between two opposite faces of the pyramid (Fig. 1a). The Berkovich indenter is typically preferred for nanoindentation or small-scale microindentation, due to the ease of preparing this three-sided pyramidal geometry on small scales compared to a four-sided pyramid [20]. The cube-corner indenter has similar, although sharper, geometry as the Berkovich indenter, and it thus induces cracking more easily [21]. While these common indenters have different geometries, giving rise to very different indentation responses, they are all made of diamond to ensure rigidity and durability of the indenters during contact with the examined glasses.

A few systematic studies of the effect of the diamond indenter geometry (e.g., varying the sharpness or number of edges) on the deformation and cracking behavior have been conducted [22–24]. Yet, the few studies do not reveal the effect of indenter geometry on all properties of interest, e.g., the crack initiation/damage resistance that is of high relevance in the development of mechanically durable glasses as justified above, hence encouraging further studies. To the authors' knowledge, it has not yet been reported how the indenter material affects the indentation response of oxide glasses. Indeed, diamond, being extremely stiff and hard, is not an ideal indenter material for mimicking real-life contact events, for which reason understanding the effect of the indenter material on the indention response is of interest. Other design parameters besides the indenter properties have previously been investigated and shown to affect the indentation response, e.g., the time of contact [25].

In this study, we systematically investigate the effect of indenter sharpness and stiffness on crack initiation and deformation in oxide glasses. We use the standard Vickers indenter and include two diamond indenters of different sharpness ($\alpha = 120°$ and $\alpha = 100°$, respectively) but otherwise same four-sided pyramid geometry as the Vickers indenter (Fig. 1b). Additionally, we include two indenters of the Vickers geometry and sharpness but made of silicon carbide and fused quartz, respectively. We perform the indentation experiments on three glasses in the sodium borosilicate system that exhibit varying degrees of densification during indentation. Our results for the variation of the indenter sharpness agree with the previous findings, and we furthermore find a relation between the indenter sharpness and the indentation size effect (ISE). We show that the crack initiation behavior is closely linked to the amount of densification and not the indenter sharpness itself. We also show that the indenter stiffness significantly affects the indentation response, especially when the stiffness of the indenter approaches that of the investigated glass. Specifically, the use of a more compliant indenter produces less visually distinct indents and reduces the propensity for crack initiation.

## 2. Experimental

### 2.1. Sample preparation

Three glasses in the sodium borosilicate system were used for this study, namely glasses of composition (in mol%) $25Na_2O$–$37.5B_2O_3$–$37.5SiO_2$ (NBS), $25Na_2O$–$75B_2O_3$ (NB), and

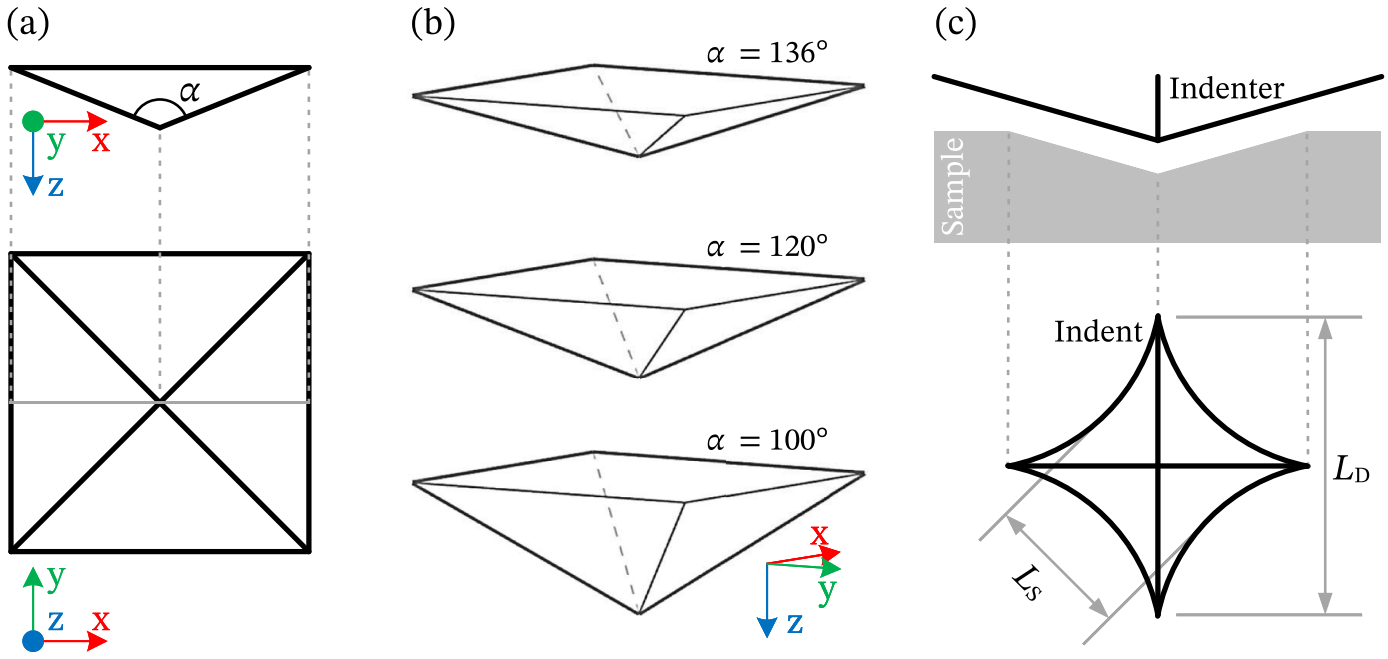


**Fig. 1.** (a) The geometry of a right square-based pyramidal indenter of tip angle $\alpha$, which is the angle between two opposite faces. (b) Three indenter geometries with tip angles $\alpha$ of 136°, 120°, and 100°, respectively, the first being the standard Vickers indenter. (c) Indentation creates an indent, whose shape to some degree resembles the indenter geometry. The formed indent has diagonal length $L_D$ and side length $L_S$ as defined in the figure.

$25Na_2O–75SiO_2$ (NS). All glasses were prepared by the traditional melt-quenching technique as described in ref. [26]. The precursors ($Na_2CO_3$, $H_3BO_3$, and $SiO_2$) were melted in an electric furnace by stepwise addition to a platinum-rhodium crucible. The melt was homogenized for ~2 h and then quenched by pouring the melt onto a brass plate. The quenched glasses were finally annealed at their respective glass transition temperature $T_g$. That is, 525 °C for NBS, 473 °C for NB, and 475 °C for NS. These values were determined previously using differential scanning calorimetry with an uncertainty of ±2 °C [26].

For the indentation experiments, samples of approximate dimensions $35 \times 20 \times 5$ mm$^3$ were cut out from the annealed glasses using a cutting machine (Secotom-10, Struers) equipped with a diamond cut-off wheel. The two largest parallel surfaces of the samples were ground using SiC grinding papers wetted with absolute ethanol, starting from grit 220 and progressively increasing the grit size to 4000. The samples were then polished to an optical finish using a polishing cloth and water-free 3 μm diamond suspension. After polishing, the samples were kept in a desiccator containing dry silica gel to minimize humid aging of the surface. Grinding with grit 4000 SiC grinding paper and polishing with the diamond suspension were repeated immediately before a sample was subjected to indentation experiments.

### 2.2. General indentation procedure

Indentation experiments with the five different indenters (Table 1) were conducted to investigate the effects on indentation cracking, hardness, and deformation mechanism. Three diamond indenters of varying sharpness (tip angle $\alpha$ of 136°, 120°, and 100°, respectively, thus the bluntest is the Vickers indenter) were used, as well as two indenters of the Vickers geometry but made of silicon carbide (SiC) and fused quartz ($SiO_2$), respectively. All indenters were purchased from Nanovea Inc. We note how silicon carbide and fused quartz are progressively less stiff and less hard compared to diamond, with the fused quartz approaching the stiffness and hardness of the investigated glasses (Table 2).

Indentation experiments were conducted using an instrumented indentation apparatus (CB500, Nanovea). Varying peak loads ($P$) in the range from 0.05 to 15 N were used. After the initial positioning of the indenter tip at the sample surface, each indentation experiment comprised a linear increase of the load from 0 to the peak load over 15 s (i.e., loading rate = peak load/(15 s)), 15 s dwell time at the peak load, and finally a linear decrease of the load to 0 over 15 s (i.e., unloading rate = loading rate). The experiment time was kept constant since keeping the loading rate constant was unfeasible without the use of very long experiment times, which in turn was because the variation in peak load was larger than two orders of magnitude. After indentation, the samples were kept in the ambient atmosphere (temperature of 22 ± 1 °C, relative humidity of 28 ± 7%) for 12–24 h, and the indents were then examined using an optical microscope (Duramin 40, Struers).

High-magnification images of the tip of all indenters were obtained based on scanning electron microscopy (SEM) imaging with an EVO LS15 (Zeiss) instrument. These measurements were done after finishing all the indentation experiments. The SEM images (Figs. S1 and S2 in the supplementary material) showed deviation from the ideal pyramidal shape at the tip of the indenters, as seen from the tip rounding. For the three diamond indenters and the SiC136° indenter, the tip rounding first became significant when the distance between the two opposing edges of the indenter was below ~0.5 μm (this distance is equivalent to the diagonal length defined for an indent in Fig. 1). For the $SiO_2$136° indenter, the tip rounding was significant for distances between two opposing edges up to ~1.5 μm. In comparison, a new $SiO_2$136° indenter was considerably less rounded at the tip, indicating small-scale deformation of the $SiO_2$136° indenter during use. This was to some degree expected, as the hardness of the $SiO_2$136° indenter material is only approximately twice that of the glasses (Table 2), and consequently, we performed a relatively low number of indentation experiments with the non-diamond indenters to minimize the potential wear of these indenters. We also continuously checked for any large-scale wear of the $SiO_2$136° indenter by visually inspecting it under a microscope, showing no wear of the indenter tip (images taken before and after use are shown in Fig. S3 in the supplementary material). In addition, after finishing the experiments, the indenter was used to produce indents under identical conditions to the initially produced indents, which showed no differences in the visual appearance or size of the indents. Thus, the small-scale wear of the $SiO_2$136° indenter tip was not found to affect the results.

Overall, we note that the tip roundness of all indenters was small compared to the size of the indents, as the indent diagonal lengths range from ~4 μm to ~90 μm. Hence, the tip roundness is not considered to be problematic, although we note it should be kept in mind for the smallest indents produced at very low peak loads (e.g., 0.05 N). Furthermore, the produced indents appear to have very limited rounding at the bottom, as seen from the atomic force microscopy (AFM) images in Figs. S4 and S5 in the supplementary material (see measurement details in Section 2.3).

**Table 1**
IDs and characteristics of the five indenters used for the present study. Indenters made of different materials and of varying sharpness (tip angle) have been used. The three indenter geometries and the definition of the tip angle $\alpha$ are shown in Fig. 1.

| Indenter ID | Tip angle, $\alpha$ | Indenter material | Note |
|---|---|---|---|
| Dia136° | 136° | Diamond | Vickers indenter |
| Dia120° | 120° | Diamond | |
| Dia100° | 100° | Diamond | |
| SiC136° | 136° | Silicon carbide | |
| $SiO_2$136° | 136° | Fused quartz | |

**Table 2**
Selected mechanical properties, including stiffness (Young's modulus) and hardness, of the indenter materials and investigated glasses.

| Material | Young's modulus, $E$ (GPa) | Poisson's ratio, $\nu$ (–) | Vickers hardness, $H_V$ (GPa) |
|---|---|---|---|
| Diamond | 1141[a] | 0.07[a] | 78[b] |
| Silicon carbide | 470[b] | 0.22[b] | 25[b] |
| Fused quartz | 72[c] | 0.17[c] | 10[d] |
| NBS glass | 75[e] | 0.24[e] | 5.6[f] |
| NB glass | 53[e] | 0.27[e] | 4.2[f] |
| NS glass | 56[e] | 0.25[e] | 4.1[f] |

[a] Data from Reference [27].
[b] Data from Reference [28].
[c] Data from Reference [29].
[d] Data from Reference [30].
[e] Data from Reference [26], the estimated errors of $E$ and $\nu$ are 2 GPa and 0.01, respectively.
[f] Data from the present study, the average standard deviation for the sampled values of $H_V$ is 0.1 GPa.

### 2.3. Indentation deformation and glass deformation mechanism

In addition to the images that were obtained by optical microscopy, the indent shapes were also assessed using AFM. For each of the five different indenters, a single indent was made on the NBS glass with a peak load of 0.3 N (corresponding to an indent diagonal of ~10 μm), and an area of 20 × 20 μm$^2$ around the indent was scanned using AFM (nGauge, ICSPI). The data were postprocessed by removing erroneous values (extreme outliers) and leveling the topography data to ensure that the background (i.e., the surface around the indents) became horizontal.

The bow-in parameter ($L_D/L_S$) and side length recovery ratio ($L_{SR}$) were measured for all combinations of glasses and indenters for indentation with a peak load of 2 N, giving insight into the deformation mechanisms of the glasses. The diagonal lengths and side lengths ($L_D$ and

$L_S$, respectively, as defined in Fig. 1c) of the indents were measured, and $L_D/L_S$ was calculated as the ratio of the diagonal length to the side length of the indents [31]. The procedure of Januchta et al. [32] was followed to find the $L_{SR}$ values, as the samples then were placed in a preheated furnace at a temperature of $0.9T_g$ (scaled in K). The samples were kept at $0.9T_g$ for 2 h and then removed from the furnace and cooled in air. The side lengths of the indents were measured again, and the side length recovery ratio ($L_{SR}$) was calculated as,

$$L_{SR} = \frac{L_{Si} - L_{Sf}}{L_{Si}}, \tag{1}$$

where $L_{Si}$ and $L_{Sf}$ are the initial side length (prior to heat treatment) and final side length (after heat treatment), respectively [32]. The reported $L_D/L_S$ and $L_{SR}$ results represent average values from several indents produced under identical conditions and analyzed independently. The number of used indents varies, as it was not always possible to accurately measure the side or diagonal lengths due to extensive cracking (e.g., formation of multiple cracks near the corners and lateral cracking), mainly occurring when using the sharp indenters. At least eight indents were used to obtain the average values of $L_D/L_S$ and $L_{SR}$, except for the indents on the NS glass made with Dia100° indenter, where only three and five indents were used to determine $L_D/L_S$ and $L_{SR}$, respectively.

For indentation on the NBS glass with a peak load of 2 N, load-displacement curves were produced for all five indenters to give insight into the indentation deformation during contact between indenter and sample. Besides recording the load ($P$) during the indentation experiments, the displacement ($h$) of the indenter relative to the glass surface was recorded by an optical non-contact depth sensor. The load-displacement data were analyzed using the method of Franco et al. [33], which is based on the Oliver-Pharr method [2]. The power-law relation $P = A(h - h_f)^m$ with the three fitting constants $A$, $h_f$, and $m$ was fitted to the unloading data from 2 N to 0.4 N. The fitted maximum displacement $h_{max}$ was calculated as $h_{max} = h_f + (P_{max}/A)^{1/m}$, where $P_{max}$ = 2 N. The stiffness $S$ (i.e., the slope of the unloading curve at maximum displacement) was then calculated as $S = mA(h_{max} - h_f)^{m-1}$. The contact depth $h_c$ was estimated as $h_c = h_{max} - 0.75P_{max}/S$ and used to calculate the estimated contact area projected on the surface, $A_c = [2\tan(\alpha/2)h_c]^2$. The reduced modulus $E_r$ was found as $E_r = 0.5062\pi^{0.5}S/A_c^{0.5}$. Finally, Young's modulus of the sample $E$ was calculated using the relation,

$$\frac{1}{E_r} = \frac{(1-\nu^2)}{E} + \frac{(1-\nu_i^2)}{E_i}, \tag{2}$$

where $\nu$ is Poisson's ratio of the sample, $\nu_i$ is Poisson's ratio of the indenter material, and $E_i$ is Young's modulus of the indenter material. The values of $\nu$, $\nu_i$, and $E_i$ were taken from Table 2. For comparison, the reduced modulus was calculated by Eq. (2) using the Young's modulus of the NBS glass as determined by ultrasonic echography ($E$ = 75 GPa, Table 2). Furthermore, the non-elastic work $W_{non\text{-}elastic}$ and elastic work $W_{elastic}$ from the load-displacement curves were calculated as described elsewhere [34]. $W_{non\text{-}elastic}$ is the area between the loading and unloading curve and $W_{elastic}$ is the area under the unloading curve. The reported results are averages of the values found by analyzing five load-displacement curves for each indenter.

### 2.4. Indentation hardness

The indentation hardness ($H$) was evaluated for all combinations of glasses and indenters. The hardness values were calculated as,

$$H = \frac{2P\sin(\alpha/2)}{{L_D}^2}, \tag{3}$$

where $P$ is the peak load, $\alpha$ is the tip angle, and $L_D$ is the diagonal length (Fig. 1). This is equivalent to the ratio of $P$ to the contact area between indenter and sample, assuming the indent has the shape of the indenter during contact and the diagonal length at maximum load is equal to the final diagonal length. As the indentation hardness is peak load-dependent due to the ISE, the indentation hardness was evaluated for peak loads of 0.1, 0.2, 0.3, 0.5, 1, 2, and 5 N for the three diamond indenters, while only for 2 N for the SiC136° and $SiO_2$136° indenters (to minimize any wear of these softer indenters). The hardness was calculated for individual indents and then averaged to obtain the reported results. As described in Section 2.3, it could be problematic to measure the diagonal lengths in some cases (due to cracking), thus a varying number of indents was used to obtain each average value. At least 10 indents were used, except for indentation with the Dia100° indenter at peak loads of 2 N (4, 13, and 6 indents for the NBS, NB, and NS glass, respectively) and 5 N (2, 5, and 5 indents for the NBS, NB, and NS glass, respectively). For the data obtained with the diamond indenters, the ISE has been quantified using the empirical relation proposed by Bernhardt [35]. The fitting parameters, $a_1$ and $a_2$, are obtained from this empirical relation by fitting the following equation to the experimental data using simple linear regression,

$$\frac{P}{L_D} = a_1 + a_2 L_D. \tag{4}$$

The $a_1$ parameter describes the extent of the ISE and $a_2$ describes the load-independent hardness. Isolating $P$ in Eq. (4) and using the expression to substitute $P$ in Eq. (3) leads to the equation,

$$H = \frac{2a_1\sin(\alpha/2)}{L_D} + 2a_2\sin(\alpha/2) = \frac{a_{ISE}}{L_D} + H_\infty, \tag{5}$$

where the parameters $a_{ISE} = 2a_1\sin(\alpha/2)$ and $H_\infty = 2a_2\sin(\alpha/2)$ have been defined, as these constants take the tip angle into account. The values of $a_{ISE}$ and $H_\infty$ were calculated from the fitted $a_1$ and $a_2$ parameters, respectively.

### 2.5. Indentation crack initiation

The indentation cracking behavior of the three glasses was investigated for the five different indenters. For the three diamond indenters, the cracking behavior was evaluated for at least six different peaks load. The range of the peak loads was adjusted for each combination of glass and indenter to ensure that peak loads with both high and low propensity for crack initiation were used. Each indentation experiment was repeated at least 20 times due to the random variation in the crack formation. The extent of cracking was quantified by calculating the crack probability ($CP$), which is defined as the ratio of the number of corner cracks to the total number of corners of the indents, i.e., $CP$ ranges from 0% to 100%. Following the approach of Wada et al. [3], the crack resistance ($CR$) is defined as the indentation peak load where $CP$ = 50%. $CR$ was estimated by fitting the equation,

$$CP(P) = \frac{100\%}{1 + (P/CR)^{-k}}, \tag{6}$$

to the experimental data, using the least squares method to optimize the fitting parameters $CR$ and $k$. For $k > 0$, the function satisfies $CP(CR)$ = 50%, $CP(\infty)$ = 100%, and the limit of $CP(P \to 0^+)$ equals 0%. The fitted function has the shape of a sigmoid function when $P$ is plotted on a logarithmic scale and is thus symmetric around $CP(CR)$, where the fitting parameter $k$ describes the steepness of the curve. This function was found to provide a better fit than a traditional sigmoid function (which features $CP(0) > 0$), especially for the low loads used for sharper indenters. To minimize the potential wear of the silicon carbide and fused quartz indenters, only four different peak loads were used for each glass and each experiment was only repeated 10 times (for loads of 0.2, 0.5, and 2 N) or five times (for loads of 5 and 10 N). Consequently, $CR$ was not estimated for the SiC136° and $SiO_2$136° indenters.

## 3. Results

### 3.1. Visual appearance of indents and indentation deformation

The indents produced with the different indenters appear visually different, as seen from the optical images in Fig. 2 for the NBS ($25Na_2O$–$37.5B_2O_3$–$37.5SiO_2$) glass. Images of the indents produced on the NB ($25Na_2O$–$75B_2O_3$) and NS ($25Na_2O$–$75SiO_2$) glasses are shown in Figs. S6 and S7, respectively, in the supplementary material. Furthermore, AFM images, showing the topography of the indentation imprint and the surrounding glass surface, are shown for indentation with the five indenters on the NBS glass in Figs. S4 and S5 in the supplementary material. The least surface damage is produced by indentation with the $SiO_2$136° indenter, while the SiC136° and Dia136° indenters induce more cracking and form more apparent indents of greater depth. Increased sharpness of the diamond indenters results in even more apparent and deeper indents and also induces more cracking. For the five different indenters, the edges between the corners of the formed four-sided indents show different degrees of inward curvature. The curvature is a result of elastic recovery of the glass [22]. The curvature is quantified by the bow-in parameter ($L_D/L_S$), which has been evaluated for the indentation with a peak load of 2 N (see Fig. 3a and Table 3). The bow-in parameters for indentation with the Dia100° indenter are close to $\sqrt{2} \approx 1.41$, i.e., the indents are almost square. Increased bow-in, hence more elastic recovery, is seen for decreased sharpness of the diamond indenters. The Dia136° and SiC136° indenters cause similar bow-in, while much higher bow-in is seen for the $SiO_2$136° indenter. We also note how $L_D/L_S$ is affected in the same way for all three glasses when using the different indenters.

The side length recovery ratio ($L_{SR}$), which has been shown to be positively correlated with the volume recovery ratio, thereby being an indirect measure of the amount of densification [32], has been determined for all indenters and glasses (Table 3 and Fig. 3b). Across all indenters, the NBS glass has the lowest $L_{SR}$ values due to its low propensity for densification, while the NB and NS glasses generally show significantly more densification upon indentation. A decrease in $L_{SR}$, hence also in the amount of densification, is observed for increased sharpness of the diamond indenters in agreement with previous findings of Yoshida et al. [23]. We also note that a larger amount of pile-up around the indent edges was observed for indentation with the sharper indenters (see the AFM images in Fig. S4 in supplementary materials), indicating that the deformation is occurring by shear flow rather than densification. The $L_{SR}$ values also show how indentation with the $SiO_2$136° indenter induces more densification compared to the Dia136° and SiC136° indenters for all glasses, including the NBS glass which generally shows limited propensity for densification.

The load-displacement curves for indentation on the NBS glass (Fig. 4, Table 4, and Fig. S8 in the supplementary material) show that a sharper diamond indenter penetrates deeper into the glass compared to a blunter indenter, resulting in more non-elastic work, while the elastic work appears almost constant as function of indenter sharpness. The deeper penetration of the sharper indenters is also evident from the AFM images of indents produced with the different indenters (Fig. S4 in the supplementary material). Furthermore, the creep during the dwell time at the peak load is progressively larger for the increased indenter sharpness. For the three diamond indenters, as expected, only minor differences are seen in the reduced moduli and Young's moduli calculated from the load-displacement curves, yet the Young's moduli and reduced moduli are consequently lower compared to the Young's modulus of 75 GPa from ultrasonic echography measurements [26] and the value of $E_{r,calculated}$, respectively (Table 4). Considering the effect of the indenter material, the load-displacement curves appear nearly identical for the Dia136° and SiC136° indenters, while the data for the SiC136° indenter show slightly larger maximum displacement and lower reduced modulus. The curve for the fused quartz indenter ($SiO_2$136°) appears very different, as the maximum displacement and elastic work are significantly larger, while the non-elastic work and reduced modulus are lower. The varying stiffness of the indenter material (Table 2) entails that the less stiff indenters will elastically deform more during contact, as also reflected in the calculated reduced modulus (Table 4), so this can directly account for the increases in maximum displacement and elastic work. As for the diamond indenters, we note that the estimated reduced moduli and Young's moduli are underestimated when compared to the calculated reduced moduli and ultrasonic echography data ($E_{NBS} = 75$ GPa).

### 3.2. Hardness and indentation size effect

The hardness values obtained with the five different indenters for an indentation peak load of 2 N are presented in Table 3 and Fig. 3c, showing that the NBS glass is significantly harder than the NB and NS glasses. The indenter material does not affect the obtained hardness values for the NB and NS glasses (Table 3 and Fig. 3c). For the NBS glass, a slight increase in apparent hardness is seen for smaller indenter stiffness, however, the increase is not large compared to the experimental error, but a plausible explanation for such a trend is discussed in Section 4.2. The finding of equal or very similar hardness values across different indenter materials is remarkable, as it illustrates how the indents produced with the Dia136°, SiC136°, and $SiO_2$136° indenters have equal or close to equal diagonal lengths despite the significant differences in the appearance of these indents (Fig. 2 and Figs. S6 and S7 in the supplementary material).

The load dependency of the measured hardness on the sharpness of the diamond indenters has also been investigated (Fig. 5). The apparent hardness seems to converge to a constant value for each glass at high loads, while differences are seen at low loads when comparing the different indenters. The indentation size effect (ISE) gives rise to higher hardness when the load decreases, but we find that the extent of the ISE effect is reduced when the indenter sharpness increases. That is, the ISE effect is largest for indentation with the Dia136° indenter and smallest for the Dia100° indenter. An empirical relation (Eq. (4)) has been fitted to obtain the two constants, $H_\infty$ and $a_{ISE}$, that describe the hardness at infinitely high loads and the magnitude of the ISE, respectively. The relation between these constants and the tip angle is shown in Fig. 6. The insets in Fig. 6 show the $a_2$ and $a_1$ parameters that are closely related to $H_\infty$ and $a_{ISE}$, respectively, as described in Section 2.4. No clear trend is seen for $H_\infty$ as it appears independent of the tip angle, while an obvious increase in $a_{ISE}$ is seen for larger tip angles (i.e., blunter indenters).

### 3.3. Indentation cracking

The cracking induced by indentation is found to greatly depend on the indenter used, as large differences are seen for otherwise constant conditions when only changing the indenter sharpness or stiffness (Fig. 2 and Figs. S6 and S7 in the supplementary material). However, all combinations of glasses and indenters feature the typical cracking behavior of so-called "normal" glasses [1]. That is, no cracking is observed for the lowest indentation peak loads, but increased load causes the formation of cracks emanating from the corners of the indents (radial/half-penny cracks) and at even higher loads also the formation of subsurface damage (lateral cracks).

Fig. 7 shows the crack probability curves for the indentation with the five different indenters. As the curves for the diamond indenters (Fig. 7a–c) cover regions with both low ($CP \approx 0\%$) and high ($CP \approx 100\%$) propensity for crack initiation, the $CR$ values have been estimated for these indenters (Table 3 and Fig. 8a). Increased indenter sharpness (i.e., lower tip angle) decreases the crack resistance, i.e., cracks are formed at lower loads. Furthermore, it is seen that a sharper indenter generally leads to a narrower transition region between the region with no crack initiation and the region with full crack initiation. Regarding the indenters of constant geometry but varying stiffness

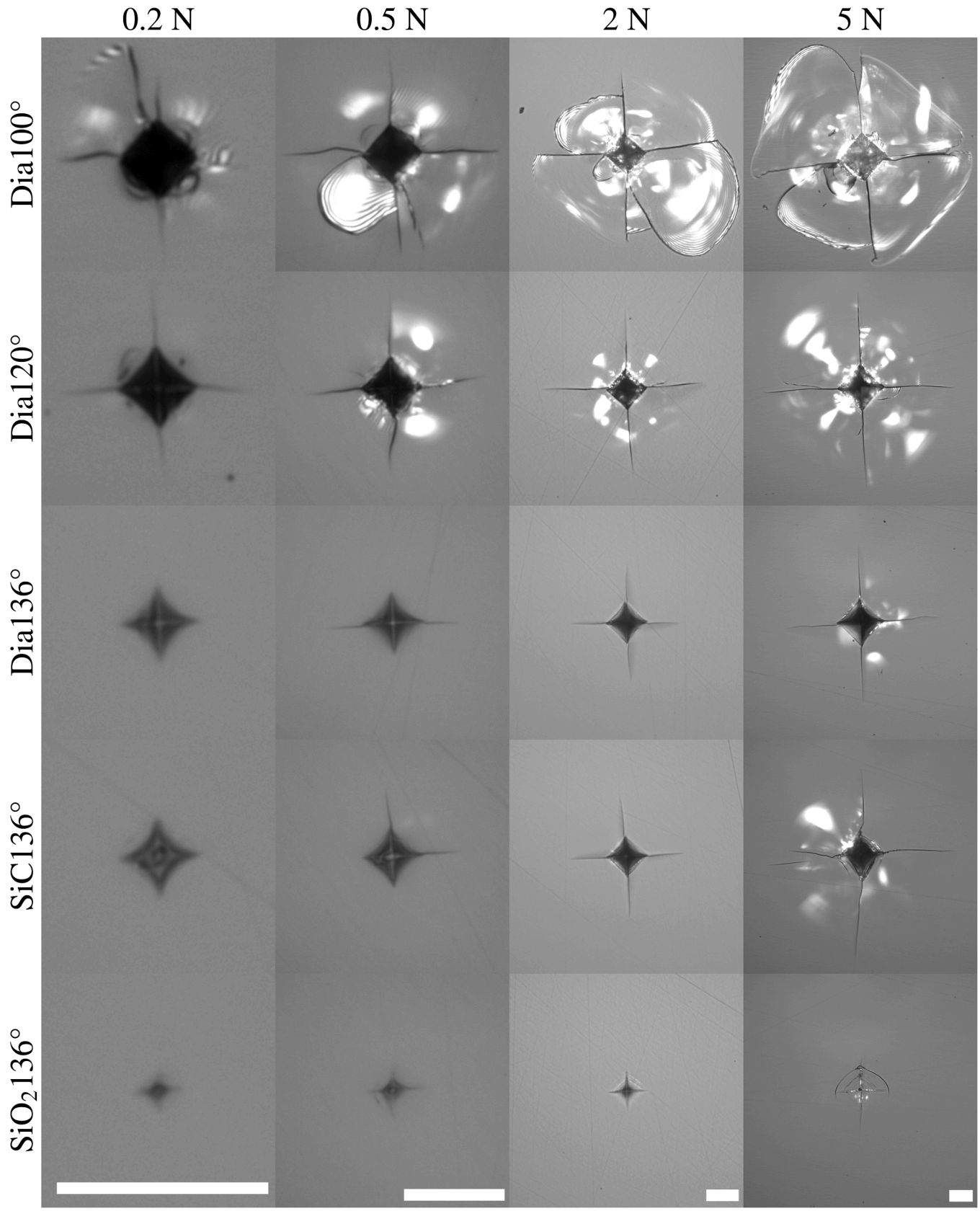


**Fig. 2.** Optical images of indents produced using different indenters and peak loads on the NBS glass of composition $25Na_2O–37.5B_2O_3–37.5SiO_2$. The white scale bar in the lower right corner of each column indicates a length of 20 μm for all images in the column.

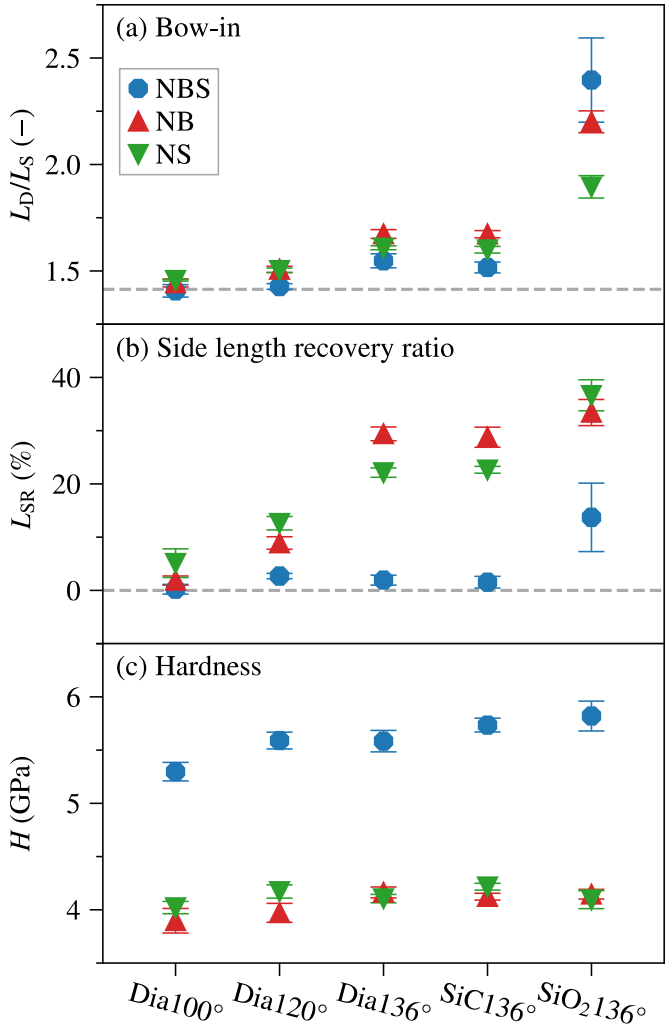


**Fig. 3.** (a) Bow-in parameter $L_D/L_S$, (b) side length recovery ratio $L_{SR}$, and (c) hardness $H$ values for indentation with different indenters (see explanation of indenter IDs in Table 1) using a fixed indentation peak load of 2 N. The values are shown for the three glasses in the study (NBS, NB, and NS) and the error bars indicate the standard deviation. In (a), the horizontal dashed line represents $\sqrt{2}$ that corresponds to no bow-in, i.e., a square indent.

(Fig. 7d–f), we observe very similar crack probability curves for the Dia136° and SiC136° indenters. However, a pronounced difference is found for the $SiO_2$136° indenter, as higher loads are required to cause crack initiation. This reveals a large increase in the crack initiation resistance, but exact *CR* values could not be determined for these non-diamond indenters due to the limited number of used loads. Besides changes in the crack initiation probability, we also note a variation in the length of the formed corner cracks when using different indenters (Fig. 2 and Figs. S6 and S7 in the supplementary material). For the diamond indenters, increased sharpness leads to longer cracks. For the indenters of different materials, the diamond and silicon carbide indenters produce cracks of similar lengths, while the use of the fused quartz indenter results in shorter cracks.

## 4. Discussion

### 4.1. Effect of indenter sharpness on cracking behavior

We have observed that the indenter sharpness has a major effect on the crack formation, with increased sharpness leading to smaller crack resistance and longer corner cracks, in agreement with the observations of Gross et al. [22,36] on different oxide glasses. Fig. 8a shows a general decrease in *CR* with decreased tip angle, yet large differences are seen in the trends when comparing the three glasses. By plotting *CR* as a function of $L_{SR}$ (Fig. 8b), we find an improved correlation between the parameters, indicating that densification (as measured by $L_{SR}$) is largely controlling the variation in *CR* when varying the indenter sharpness. We note that $L_{SR}$, or densification in general, is not the only controlling factor for *CR* when comparing glasses of different compositions [32], but here it describes the variation in *CR* with indenter sharpness well.

**Table 3**
Bow-in parameter ($L_D/L_S$), side length recovery ratio ($L_{SR}$), indentation hardness ($H$), and crack resistance ($CR$) values for indentation with indenters of varying tip angles and different materials. The data is presented for the NBS, NB, and NS glasses (see Section 2.1). An indentation peak load of 2 N was used for the evaluation of $L_D/L_S$, $L_{SR}$, and $H$. The average standard deviations for $L_D/L_S$, $L_{SR}$, and $H$ are 0.03, 2%, and 0.1 GPa, respectively, and the estimated error for *CR* is 20% of the value.

| | | Dia100° | Dia120° | Dia136° | SiC136° | $SiO_2$136° |
|---|---|---|---|---|---|---|
| $L_D/L_S$ (–) | NBS | 1.41 | 1.43 | 1.55 | 1.52 | 2.40 |
| | NB | 1.44 | 1.51 | 1.67 | 1.67 | 2.20 |
| | NS | 1.46 | 1.50 | 1.61 | 1.60 | 1.90 |
| $L_{SR}$ (%) | NBS | 0 | 3 | 2 | 2 | 14 |
| | NB | 2 | 9 | 29 | 29 | 33 |
| | NS | 5 | 13 | 22 | 23 | 37 |
| $H$ (GPa) | NBS | 5.3 | 5.6 | 5.6 | 5.7 | 5.8 |
| | NB | 3.9 | 4.0 | 4.2 | 4.1 | 4.1 |
| | NS | 4.0 | 4.2 | 4.1 | 4.2 | 4.1 |
| *CR* (N) | NBS | 0.12 | 0.13 | 0.59 | – | – |
| | NB | 0.21 | 0.29 | 4.7 | – | – |
| | NS | 0.50 | 2.8 | 4.7 | – | – |

### 4.2. Effect of indenter stiffness on indentation response

We have shown that the indenter material can have a profound effect on the indentation response of the investigated glasses. However, we have not observed any significant differences in the indentation responses when comparing the diamond and silicon carbide indenters of the Vickers geometry. The hardness and stiffness of diamond and silicon carbide differ significantly, yet both materials are much harder and stiffer than the investigated glasses (Table 2). Hence, the Dia136° and SiC136° indenters experience no or little elastic and permanent deformation during indentation, thus they can be considered rigid. Therefore, identical or very similar indentation responses are observed when using these two indenters.

On the contrary, the mechanical properties of fused quartz are much more like those of the investigated oxide glasses. The stiffness (Young's modulus) of fused quartz is in the same range as that of the NBS, NB, and NS glasses, while its Vickers hardness is roughly two times higher than those of the investigated glasses (Table 2). Due to its higher hardness, only very limited permanent deformation of the $SiO_2$136° (fused quartz) indenter was observed in this study (see Section 2.2), and this deformation occurred on a smaller scale than the size of the produced indents. Thus, permanent deformation of the $SiO_2$136° indenter cannot account for large differences in the indentation response. However, significant elastic deformation of the $SiO_2$136° indenter has occurred during indentation due to its stiffness being similar to those of the investigated glasses, which was also expected considering the calculated reduced modulus in Table 4. The elastic deformation of the indenter is evident from the load-displacement curves (Fig. 4), the elastic work, and the measured reduced moduli (Table 4). Compared to the Dia136° and SiC136° indenters, the load-displacement curve for the $SiO_2$136° indenter shows lower final displacement in agreement with the formation of a shallower indent for this indenter (see AFM images in Fig. S5 in the supplementary material). As such, the larger maximum

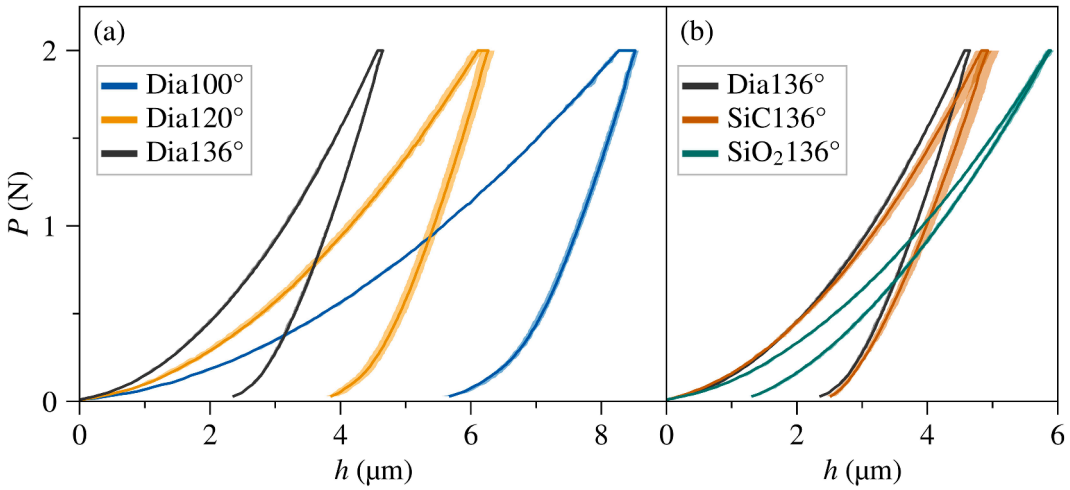


**Fig. 4.** Load-displacement (*P-h*) curves for indentation on the NBS glass with indenters of (a) varying sharpness and (b) different materials. A constant peak load of 2 N was used. The solid lines represent the average of five repetitions, while the full range of the five repetitions is shown with a lighter color for each indenter. Fig. S8 in the supplementary material shows the same curves horizontally shifted so that the points of maximum displacement are aligned.

**Table 4**
Maximum displacement ($h_{max}$), non-elastic work ($W_{non\text{-}elastic}$), elastic work ($W_{elastic}$), reduced modulus ($E_{r,measured}$), and Young's modulus ($E$) calculated from the load-displacement curves for indentation on the NBS glass with the five different indenters using an indentation peak load of 2 N. The average standard deviations of $h_{max}$, $W_{non\text{-}elastic}$, $W_{elastic}$, $E_{r,measured}$, and $E$ are 0.05 μm, 0.03 μJ, 0.03 μJ, 1 GPa, and 2 GPa, respectively. Furthermore, reduced modulus values ($E_{r,calculated}$) calculated with Eq. (2) and the data in Table 2 are shown.

| | Dia100° | Dia120° | Dia136° | SiC136° | $SiO_2$136° |
|---|---|---|---|---|---|
| $h_{max}$ (μm) | 8.52 | 6.26 | 4.64 | 4.92 | 5.88 |
| $W_{non\text{-}elastic}$ (μJ) | 4.69 | 2.95 | 1.64 | 1.77 | 0.65 |
| $W_{elastic}$ (μJ) | 1.89 | 1.79 | 1.79 | 2.01 | 3.77 |
| $E_{r,measured}$ (GPa) | 67 | 67 | 69 | 59 | 33 |
| $E_{r,calculated}$ (GPa) | 74 | 74 | 74 | 69 | 39 |
| $E$ (GPa) | 67 | 68 | 69 | 63 | 57 |

displacement observed from the load-displacement curve for the $SiO_2$136° indenter is not a result of deeper penetration into the glass, but instead a result of elastic compaction of the indenter itself. We note how the increased elastic work (Table 4) and the larger displacement of the unloading curve show that this displacement is elastic. Thus, the use of the $SiO_2$136° indenter gives different indentation responses compared to the stiffer indenters due to the deformation of the fused quartz indenter, thereby changing the indenter geometry during contact with the sample.

Compared to the Dia100°, Dia120°, and Dia136° indenters, we note that the results obtained with the $SiO_2$136° indenter fit the trends as a diamond indenter with a tip angle larger than 136°, i.e., an even blunter diamond indenter. This is seen from the values of $L_D/L_S$ (Fig. 3a), $L_{SR}$ (Fig. 3b), crack initiation resistance (Fig. 7), lengths of formed cracks (Fig. S6 in the supplementary information), and the depth of the indents (Figs. S4 and S5 in the supplementary information). That is, the use of a compliant indenter that deforms elastically during indentation appears to reduce the effective sharpness of the indenter. This is supported by the similarities between the indents produced with the $SiO_2$136° indenter and the indents produced by Gross [22] using a diamond indenter with a tip angle of 160° as shown in Fig. 9. The shown indents were produced on two different glasses and using slightly different peak loads, yet the indentation responses appear very similar for the Vickers (Dia136°) indenters, thereby justifying the comparison.

The effect of the relatively low stiffness of the $SiO_2$136° indenter on the indentation response (e.g., visual appearance of the indents, bow-in, and side length recovery ratio) is more pronounced for the NBS glass compared to the NB and NS glasses. This is because the NBS glass is the stiffest of the three glasses, in fact slightly stiffer than fused quartz (Table 2), i.e., the $SiO_2$136° indenter is deformed most for this glass, whereas deformation of this indenter occurs to a smaller extent for the more compliant NB and NS glasses.

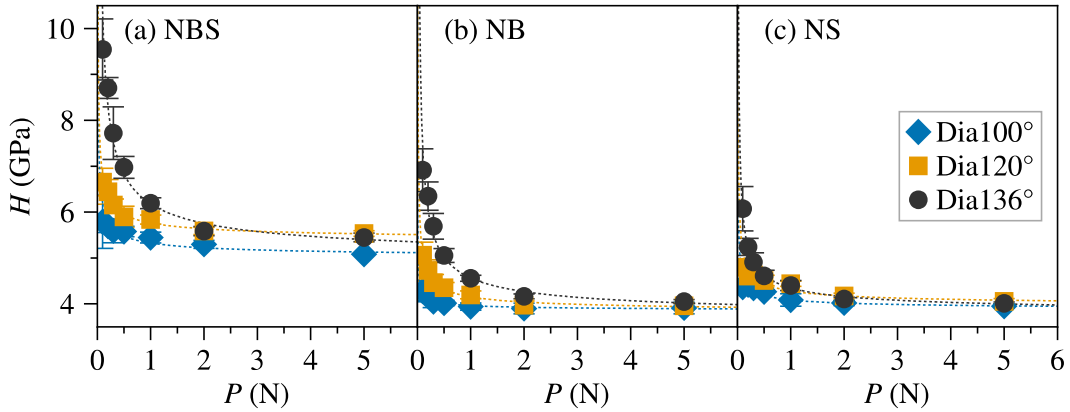


**Fig. 5.** Load dependence of hardness (*H*) for indentation with the three different diamond indenters of varying sharpness on the NBS, NB, and NS glasses. The error bars represent the standard deviation. The dotted lines represent the fit of the model in Eq. (5), where the used parameters were obtained by fitting Eq. (4) to the data as described in Section 2.4.

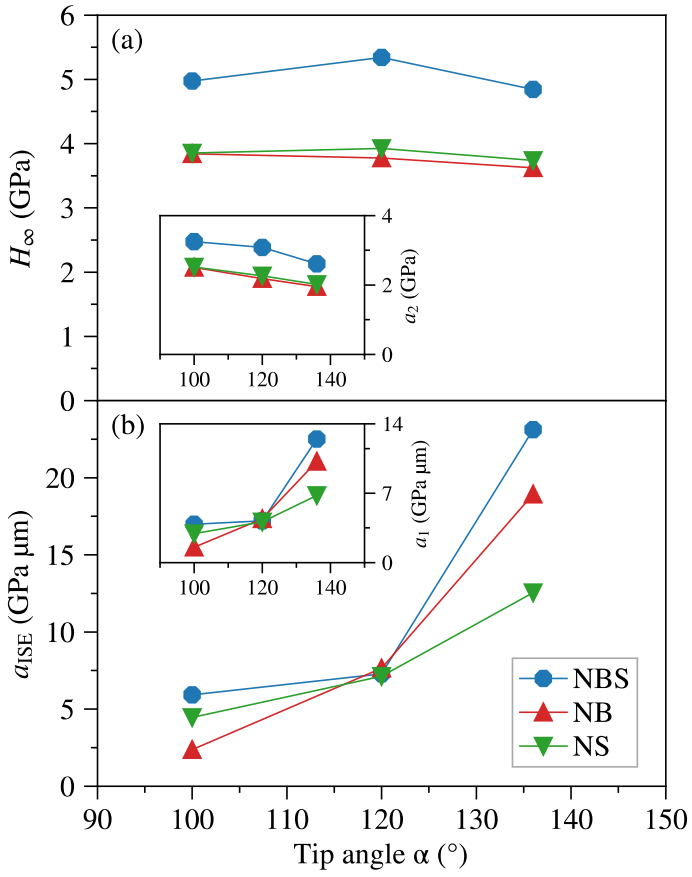


**Fig. 6.** Tip angle dependence of (a) $H_\infty$ and (b) $a_{ISE}$ for the three glasses. The insets show the (a) $a_2$ and (b) $a_1$ parameters that have been determined by fitting Eq. (4) to the experimental data, and then used to calculate $H_\infty$ and $a_{ISE}$ as described in Section 2.4. $H_\infty$ is the load-independent hardness (i.e., the hardness at infinitely high load) and $a_{ISE}$ is a measure of the extent of the indentation size effect.

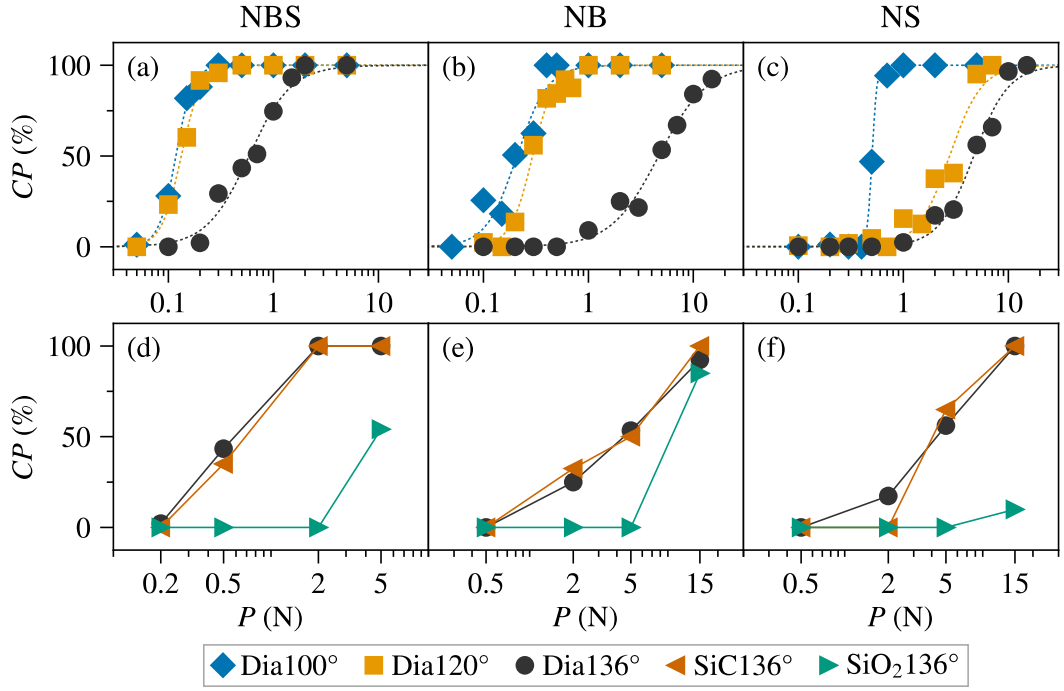


**Fig. 7.** Crack probability (*CP*) vs. load (*P*) curves for indentation on the NBS, NB, and NS glasses with the five different indenters (Table 1). Figures a-c show the curves for indentation with three diamond indenters of varying sharpness, to which Eq. (6) has been fitted (dotted lines) to determine the crack resistance (*CR*) values. Figures d-f show the *CP* values measured at four loads using indenters of different materials but identical geometry (Dia136°, SiC136°, and $SiO_2$136°).

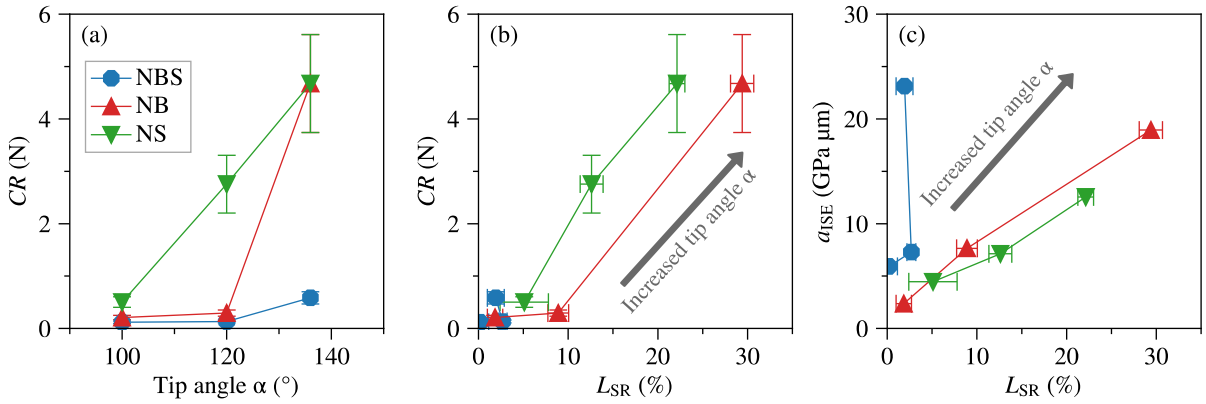


**Fig 8.** Relations between selected indentation properties for the diamond indenters of varying sharpness (tip angle). (a) Crack resistance *CR* plotted against tip angle $\alpha$. (b) *CR* against side length recovery ratio $L_{SR}$. (c) The $a_{ISE}$ parameter (describing the extent of the ISE) against $L_{SR}$. The error bars for $L_{SR}$ indicate the standard deviation, whereas the error bars for *CR* indicate the estimated error of 20% of the *CR* value.

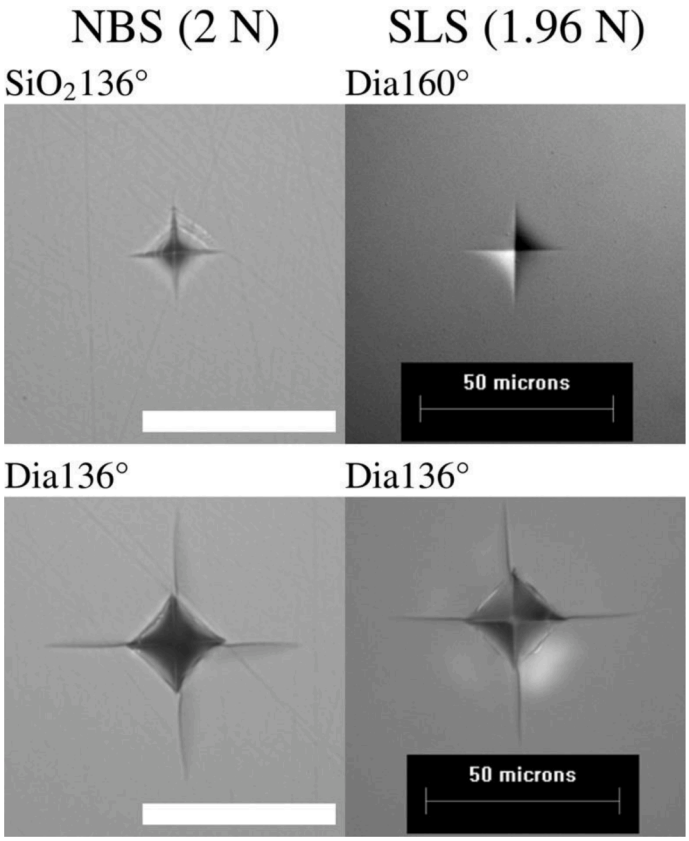


**Fig. 9.** Left: Indents made on the NBS glass in this study with the $SiO_2$136° indenter and the Dia136° (Vickers) indenter, respectively. Right: Images reproduced from Gross [22] with permission of Elsevier, showing indents made on a soda-lime silicate (SLS) glass with a pyramidal diamond indenter of 160° tip angle (i.e., Dia160° following the naming used in Table 1) and a Vickers indenter (i.e., Dia136°), respectively. As indicated, the used peak load was 2 N for the indents in this study (left) and 1.96 N for the indents made by Gross (right). All four scale bars indicate a length of 50 µm.

Lastly, we note that the trend of increased apparent hardness with lower indenter stiffness for the NBS glass (see Section 3.2 and Fig. 3c) agrees with the concept of reduced effective sharpness of less stiff indenters. That is, the lower effective sharpness of the $SiO_2$136° indenter causes the extent of the ISE to increase (see trend in Figs. 5 and 6b), thereby giving a small increase in apparent hardness at 2 N where the ISE is present but still small compared to lower load values (Fig. 5). No observable increase in apparent hardness with reduced indenter stiffness is seen for the NB and NS glasses (Fig. 3c), since the effect is most pronounced for the NBS glass compared to the NS and NB glasses as described above.

### 4.3. Effect of indenter sharpness on hardness measurements

We have established that indenter sharpness affects the measured hardness by changing the magnitude of the ISE (as characterized by $a_{ISE}$), while the load-independent hardness ($H_\infty$) remains unaffected. First, this knowledge is useful for understanding the origin of the ISE. Several ideas have been proposed to describe the origin of the ISE, e.g., by ascribing it to surface energy [35], cracking [37], or friction [38]. Yet, a satisfactory understanding of the ISE in oxide glasses is still lacking [39,40]. Here, we find an increase in the $a_{ISE}$ parameter with increasing tip angle for all three glasses (Fig. 6b). We also observe an overall increase in *CR* with tip angle, but *CR* is found to correlate with the amount of densification and not the tip angle itself (Fig. 8a-b). Interestingly, $a_{ISE}$ behaves differently as the NBS glass also exhibits a

high $a_{ISE}$ value for indentation with the blunt Vickers indenter despite showing only a small amount of densification (Fig. 8c). Thus, $a_{ISE}$ correlates better with the tip angle relative to the amount of indentation-induced densification. As such, a general theory on the ISE in oxide glasses should be able to account for the observed relation between the ISE and the indenter sharpness.

Second, we emphasize that sharper indenters than the Vickers indenter provide hardness measurements that are less load-dependent (see Figs. 5 and 6). Thus, markedly lower indentation loads can be used without the hardness measurements being significantly affected by the ISE. Hence, for small or thin samples where relatively large indentation loads cannot be used, the use of a sharp indenter is a convenient way of minimizing the ISE to obtain a hardness value close to the load-independent value $H_\infty$. We also note that $H_\infty$ is found to be independent of the indenter sharpness (for four-sided pyramidal geometries), thus measured hardness values can be directly compared across indenters of different sharpness if the ISE has not affected the measurements. This indicates that it is possible to define a hardness measure that is assessed by indentation, but being independent of both the used indenter geometry and indentation load, thereby being a more intrinsic material property than the typically reported indentation hardness values.

### 4.4. Implications for experiments mimicking real-life damage formation

The findings of the present study are relevant when using the indentation technique to assess glasses' resistance to formation of surface damage that can lead to reduced strength and durability. First, we note that the indentation response appears unaffected by variations of the indenter stiffness when the indenter is considerably stiffer than the investigated glasses. Thus, diamond indenters, or other very stiff indenters, can mimic contact events with more compliant materials as long as the sample is even more compliant. When the stiffness of the indenter is only slightly higher than or similar to that of the sample, the indenter deforms significantly, which decreases the effective indenter sharpness. This could be relevant for indentation experiments seeking to mimic real-life contact events between materials of similar stiffness, such as the contact between glass and stone or (quartz) sand that, e.g., can happen when dropping the cover glass of a mobile device onto a rough concrete surface. In such cases, it can be reasonable to use a more durable, but stiffer, indenter material (e.g., diamond) rather than a less durable material (e.g., quartz), while accounting for the higher indenter stiffness by reducing the geometric indenter sharpness to reach the desired effective sharpness. However, further work is required to establish a quantitative relation between indenter properties and effective sharpness.

Next, we note that sharp and stiff indenters induce the most substantial surface damage, thus the most critical objects in real-life situations are expectedly the sharpest objects that are substantially stiffer than the glass. From this perspective, the practice of using a Vickers indenter, a relatively blunt indenter, for evaluation of damage resistance could be questioned. Furthermore, for contact with objects sharper than a Vickers indenter, the densification mechanism is progressively shut down, in turn reducing the crack initiation resistance. Thus, developing glasses with high Vickers crack resistance by increasing the amount of densification might be ineffective for increasing the real-life performance if the densification does not affect the crack resistance for sharp contact events.

## 5. Conclusions

We have studied the response of oxide glasses to instrumented indentation testing with indenters of varying sharpness and stiffness. For four-sided pyramid diamond indenters, increased sharpness leads to increased propensity for crack initiation as densification deformation decreases. With increased indenter sharpness, more pile-up is also seen around the indents because shear flow is favored compared to densification as the deformation mechanism. Indenter sharpness also affects the hardness measurements, as although the hardness values at relatively high loads are independent of the indenter sharpness, the magnitude of the indentation size effect is reduced with increased indenter sharpness. For indenters with Vickers-type geometry, changing the indenter material does not significantly affect the indentation response when the indenter material is substantially stiffer and harder than the sample. However, the indentation response is remarkably different for a fused quartz indenter, as elastic deformation of the indenter reduces its effective sharpness and affects the indentation response accordingly. This understanding of the indenter sharpness and indenter material effects is important for proper design of indentation experiments and interpretations of the results, e.g., when mimicking real-life contact events or assessing the real-life damage resistance.

## CRediT authorship contribution statement

**Johan F.S. Christensen:** Conceptualization, Investigation, Writing – original draft. **N.M. Anoop Krishnan:** Writing – review & editing. **Mathieu Bauchy:** Writing – review & editing. **Morten M. Smedskjaer:** Conceptualization, Supervision, Writing – review & editing.

## Declaration of Competing Interest

The authors declare that they have no known competing financial interests or personal relationships that could have appeared to influence the work reported in this paper.

## Data Availability

Data will be made available on request.

## Acknowledgments

We thank Kacper Januchta, Lars R. Jensen, Nadja Lönnroth, Søren S. Sørensen, Theany To, and Thomas S. Quaade for experimental assistance and/or helpful discussions. This work is supported by funding from the Poul Due Jensen Foundation (Grundfos Prize). M.B. acknowledges funding from the National Science Foundation under grants CMMI-1826420 and DMR-1928538.

## Supplementary materials

Supplementary material associated with this article can be found, in the online version, at doi:10.1016/j.jnoncrysol.2022.122111.

## References

[1] J.P. Guin, Y. Gueguen, Mechanical properties of glass, in: J.D. Musgraves, J. Hu, L. Calvez (Eds.). Springer Handbook of Glass, Springer, Cham, 2019, pp. 227–271, https://doi.org/10.1007/978-3-319-93728-1.
[2] W.C. Oliver, G.M. Pharr, An improved technique for determining hardness and elastic modulus using load and displacement sensing indentation experiments, J. Mater. Res. 7 (1992) 1564–1583, https://doi.org/10.1557/JMR.1992.1564.
[3] M. Wada, H. Furukawa, K. Fujita, Crack resistance of glass on Vickers indentation, in: M. Kunigi, M. Tashiro, N. Saga (Eds.), Proceedings of the 10th International Congress on Glass, vol. 11, Ceramic Society of Japan, Kyoto, 1974, pp. 39–46.
[4] S. Yoshida, J.C. Sanglebœuf, T. Rouxel, Quantitative evaluation of indentation-induced densification in glass, J. Mater. Res. 20 (2005) 3404–3412, https://doi.org/10.1557/jmr.2005.0418.
[5] K. Januchta, M.M. Smedskjaer, Indentation deformation in oxide glasses: quantification, structural changes, and relation to cracking, J. Non-Cryst. Solids X 1 (2019), 100007, https://doi.org/10.1016/j.nocx.2018.100007.
[6] T. Rouxel, J. Jang, U. Ramamurty, Indentation of glasses, Prog. Mater. Sci. 121 (2021), 100834, https://doi.org/10.1016/j.pmatsci.2021.100834.
[7] S. Yoshida, Indentation deformation and cracking in oxide glass –toward understanding of crack nucleation, J. Non-Cryst. Solids X 1 (2019), 100009, https://doi.org/10.1016/j.nocx.2019.100009.

[8] T.K. Bechgaard, J.C. Mauro, M.M. Smedskjaer, Time and humidity dependence of indentation cracking in aluminosilicate glasses, J. Non-Cryst. Solids 491 (2018) 64–70, https://doi.org/10.1016/j.jnoncrysol.2018.04.009.
[9] T. Rouxel, Driving force for indentation cracking in glass: composition, pressure and temperature dependence, Philos. Trans. R. Soc. A 373 (2015), 20140140, https://doi.org/10.1098/rsta.2014.0140.
[10] L. Wondraczek, E. Bouchbinder, A. Ehrlicher, J.C. Mauro, R. Sajzew, M. M. Smedskjaer, Advancing the mechanical performance of glasses: perspectives and challenges, Adv. Mater. 34 (2022), 2109029, https://doi.org/10.1002/adma.202109029.
[11] L. Wondraczek, J.C. Mauro, J. Eckert, U. Kühn, J. Horbach, J. Deubener, T. Rouxel, Towards ultrastrong glasses, Adv. Mater. 23 (2011) 4578–4586, https://doi.org/10.1002/adma.201102795.
[12] A.K. Varshneya, Stronger glass products: lessons learned and yet to be learned, Int. J. Appl. Glass Sci. 9 (2018) 140–155, https://doi.org/10.1111/ijag.12341.
[13] G.D. Quinn, R.C. Bradt, On the Vickers indentation fracture toughness test, J. Am. Ceram. Soc. 90 (2007) 673–680, https://doi.org/10.1111/j.1551-2916.2006.01482.x.
[14] J.J. Price, G.S. Glaesemann, D.A. Clark, T.M. Gross, K.L. Barefoot, 69.3: A mechanics framework for ion-exchanged cover glass with a deep compression layer, SID Symp. Dig. Tech. Pap. 40 (2009) 1049–1051, https://doi.org/10.1889/1.3256467.
[15] K. Januchta, R.E. Youngman, A. Goel, M. Bauchy, S.L. Logunov, S.J. Rzoska, M. Bockowski, L.R. Jensen, M.M. Smedskjaer, Discovery of ultra-crack-resistant oxide glasses with adaptive networks, Chem. Mater. 29 (2017) 5865–5876, https://doi.org/10.1021/acs.chemmater.7b00921.
[16] K. Januchta, M. Stepniewska, L.R. Jensen, Y. Zhang, M.A.J. Somers, M. Bauchy, Y. Yue, M.M. Smedskjaer, Breaking the limit of micro-ductility in oxide glasses, Adv. Sci. 6 (2019), 1901281, https://doi.org/10.1002/advs.201901281.
[17] Corning Incorporated, Corning® Gorilla® Glass 3, https://www.corning.com/microsites/csm/gorillaglass/PI_Sheets/2020/Gorilla_Glass_3_ProdSheet.pdf, 2020 (accessed 10 May 2022).
[18] A.K. Varshneya, J.C. Mauro. Fundamentals of Inorganic Glasses, 3rd ed., Elsevier, Amsterdam, 2019 https://doi.org/10.1016/C2017-0-04281-7.
[19] ASTM E384-17, Standard Test Method for Microindentation Hardness of Materials, ASTM International, West Conshohocken, 2017, https://doi.org/10.1520/E0384-17.
[20] A.C. Fischer-Cripps, Introduction to Contact Mechanics, 2nd ed., Springer, New York, 2007 https://doi.org/10.1007/978-0-387-68188-7.
[21] D.J. Morris, R.F. Cook, *In situ* cube-corner indentation of soda-lime glass and fused silica, J. Am. Ceram. Soc. 87 (2004) 1494–1501, https://doi.org/10.1111/j.1551-2916.2004.01494.x.
[22] T.M. Gross, Deformation and cracking behavior of glasses indented with diamond tips of various sharpness, J. Non-Cryst. Solids 358 (2012) 3445–3452, https://doi.org/10.1016/j.jnoncrysol.2012.01.052.
[23] S. Yoshida, H. Sawasato, T. Sugawara, Y. Miura, J. Matsuoka, Effects of indenter geometry on indentation-induced densification of soda-lime glass, J. Mater. Res. 25 (2010) 2203–2211, https://doi.org/10.1557/jmr.2010.0287.
[24] S. Yoshida, K. Wada, T. Fujimura, A. Yamada, M. Kato, J. Matsuoka, N. Soga, Evaluation of sinking-in and cracking behavior of soda-lime glass under varying angle of trigonal pyramid indenter, Front. Mater. 3 (2016) 54, https://doi.org/10.3389/fmats.2016.00054.
[25] T.M. Gross, J.J. Price, Vickers indentation cracking of ion-exchanged glasses: quasi-static vs. dynamic contact, Front. Mater. 4 (2017) 4, https://doi.org/10.3389/fmats.2017.00004.
[26] K. Januchta, T. To, M.S. Bødker, T. Rouxel, M.M. Smedskjaer, Elasticity, hardness, and fracture toughness of sodium aluminoborosilicate glasses, J. Am. Ceram. Soc. 102 (2019) 4520–4537, https://doi.org/10.1111/jace.16304.
[27] J.E. Field, C.S.J. Pickles, Strength, fracture and friction properties of diamond, Diam. Relat. Mater. 5 (1996) 625–634, https://doi.org/10.1016/0925-9635(95)00362-2.
[28] F. Cardarelli, Materials Handbook, 3rd ed., Springer, Cham, 2018 https://doi.org/10.1007/978-3-319-38925-7.
[29] General Electric Fused Quartz Products Technical Data, general catalog number 7705-7725, April 1985.
[30] Nanovea Inc., personal communication with manufacturer, 2021.
[31] S. Yoshida, M. Kato, A. Yokota, S. Sasaki, A. Yamada, J. Matsuoka, N. Soga, C. R. Kurkjian, Direct observation of indentation deformation and cracking of silicate glasses, J. Mater. Res. 30 (2015) 2291–2299, https://doi.org/10.1557/jmr.2015.214.
[32] K. Januchta, P. Liu, S.R. Hansen, T. To, M.M. Smedskjaer, Indentation cracking and deformation mechanism of sodium aluminoborosilicate glasses, J. Am. Ceram. Soc. 103 (2020) 1656–1665, https://doi.org/10.1111/jace.16894.
[33] A.R. Franco Jr., G. Pintaúde, A. Sinatora, C.E. Pinedo, A.P. Tschiptschin, The use of a Vickers indenter in depth sensing indentation for measuring elastic modulus and Vickers hardness, Mater. Res. 7 (2004) 483–491, https://doi.org/10.1590/S1516-14392004000300018.
[34] M. Stepniewska, K. Januchta, C. Zhou, A. Qiao, M.M. Smedskjaer, Y. Yue, Observation of indentation-induced shear bands in a metal−organic framework glass, PNAS 117 (2020) 10149–10154, https://doi.org/10.1073/pnas.2000916117.
[35] E.O. Bernhardt, Über die Mikrohärte der Feststoffe im Grenzbereich des Kick'schen Ähnlichkeitssatzes, Z. Metallkunde 33 (1941) 135–144.
[36] T.M. Gross, H. Liu, Y. Zhai, L. Huang, J. Wu, The impact of densification on indentation fracture toughness measurements, J. Am. Ceram. Soc. 103 (2020) 3920–3929, https://doi.org/10.1111/jace.16793.
[37] M. Swain, M. Wittling, Indentation size effects for brittle materials: is there a simple fracture mechanics explanation, in: R.C. Bradt, D.P.H. Hasselman, D. Munz, M. Sakai, V.Y. Shevchenko (Eds.), Fracture Mechanics of Ceramics, vol. 11, Plenum Press, New York, 1996, pp. 379–388.
[38] H. Li, R.C. Bradt, The indentation load/size effect and the measurement of the hardness of vitreous silica, J. Non-Cryst. Solids 146 (1992) 197–212, https://doi.org/10.1016/S0022-3093(05)80492-2.
[39] T.M. Gross, M. Tomozawa, Fictive temperature-independent density and minimum indentation size effect in calcium aluminosilicate glass, J. Appl. Phys. 104 (2008), 063529, https://doi.org/10.1063/1.2985907.
[40] M. Kazembeyki, M. Bauchy, C.G. Hoover, New insights into the indentation size effect in silicate glasses, J. Non-Cryst. Solids 521 (2019), 119494, https://doi.org/10.1016/j.jnoncrysol.2019.119494.